JOURNAL OF SOLID STATE CHEMISTRY 115, 98–111 (1995)

Synthesis, Structural Study, and Magnetic Behavior of a New Chlorofluoride Family: $Ba_2M_2F_7Cl$ and $Ba_2MM'F_7Cl$ (M, M' = Mn^{2+}, Fe^{2+}, Co^{2+}, Ni^{2+}, Zn^{2+})

J-J. Maguer and G. Courbion[1]

Laboratoire des Fluorures, URA CNRS 449, Faculté des Sciences, Université du Maine, 72017 Le Mans Cedex, France

and

M. S. Schriewer-Pöttgen,[2] J. Fompeyrine, and J. Darriet

Laboratoire de Chimie du Solide du CNRS, Université Bordeaux I, 351, Cours de la Libération, 33405 Talence Cedex, France

Received March 30, 1994; in revised form June 8, 1994; accepted June 13, 1994

A new chlorofluoride series, $Ba_2M_2F_7Cl$ and $Ba_2MM'F_7Cl$ (M^{2+}, M'^{2+} = Mn^{2+}, Fe^{2+}, Co^{2+}, Ni^{2+}, Zn^{2+}), has been discovered. Structure determinations were achieved in the monoclinic $P2_1/m$ space group ($Z = 2$) for two single crystals with the following cell parameters: (1) $Ba_2Zn_2F_7Cl$ (a = 7.700(2) Å, b = 5.801(2) Å, c = 8.939(2) Å, β = 106.85(2)°) and (2) $Ba_2Co_2F_7Cl$ (a = 7.692(3) Å, b = 5.783(2) Å, c = 8.945(2) Å, β = 106.88(2)°). The reliability factors are respectively $R_{(1)} = 0.028$, $R_w(1) = 0.032$ (for 795 structure factors and 65 refined parameters) and $R_{1(2)} = 0.036$, $wR_{2(2)} = 0.044$ (for 1065 structure factors and 64 refined parameters). The structure is built up from (MF_5Cl) octahedra, sharing vertices in order to form puckered $[MX_4]$ layers. A cationic order is possible for the the Ba_2MnNiF_7Cl compound. The structure is compared to the $BaZnF_4$ and $NaCrF_4$ structure types. The magnetic measurements on the full series exhibit an antiferromagnetic behavior (except for the Zn family), as usually encountered in two-dimensional structures.

INTRODUCTION

Inorganic solid fluorides have been investigated intensively in the past because of their interesting crystal chemistry and their magnetic properties (see for example Ref. (1) and references therein). In contrast, little information is available on the crystal chemistry of chlorofluorides: around 20 crystal structure determinations have been reported up to now (from the Inorganic Crystal Structure Database (ICSD) (2)). The more recent structure determinations (involving 3d cations or Al) are $K_2Cr_3F_6Cl_2$ (3), $Sr_{10}Al_2F_{25}Cl$ (4), and $K_3Ba_7Al_6F_{33}Cl_2$ (5). Consequently, few physical properties have been pointed out. As we are particularly interested in the magnetic properties of compounds involving 3d cations, we began investigations in the (Ba, M, M')–(F, Cl) system, M and M' being divalent 3d transition cations. In this system, besides the chlorofluorides BaFCl (6) and Ba_2F_3Cl (7), only $Ba_2Mn_2ZnF_{12}Cl_6$ (8) has been reported.

The present paper is devoted to the structure determinations of $Ba_2Zn_2F_7Cl$, $Ba_2Co_2F_7Cl$, and Ba_2MnNiF_7Cl, and then to the magnetic behavior of both $Ba_2M_2F_7Cl$ and $Ba_2MM'F_7Cl$ series (the crystal structure determinations of the zinc and cobalt compounds were performed concomitantly in the two laboratories).

SYNTHESIS AND EXPERIMENTAL DETAILS

The solid state synthesis of the $Ba_2M_2F_7Cl$ series (M^{II} = Mn^{2+}, Fe^{2+}, Co^{2+}, Ni^{2+}, Zn^{2+}) was achieved in sealed gold tubes from stoichiometric mixtures of the elementary halides (temperatures ranging between 500 and 750°C). Attempts with M^{II} = Mg^{2+}, Cr^{2+}, Cu^{2+} and trials of substituting Sr^{2+} for Ba^{2+} failed. Furthermore, we synthesized a series of 10 combined compounds $Ba_2MM'F_7Cl$ (M, M' = Mn^{2+}, Fe^{2+}, Co^{2+}, Ni^{2+}, Zn^{2+}), in order to study their crystallographic and magnetic properties.

Crystals of $Ba_2Zn_2F_7Cl$ were obtained in large quantities by using a chloride flux method (9, 10) in a platinum crucible under argon atmosphere. The initial mixture ($5ZnCl_2$ + NaF + ZnF_2 + BaF_2), slowly cooled (5°C/hr) from 550°C, allowed the synthesis of parallelepipedic crystals which were easily differentiated from impurities,

[1] To whom correspondence should be addressed.

[2] Permanent address: Anorganisch-Chemisches Institut, Universität Münster, Wilhelm Klemm-Strasse 8, D-48149 Münster, Germany.

0022-4596/95 $6.00

mainly composed of crystals of BaFCl in the form of platelets. An EDX analysis, performed with a JEOL-2010 TEM equipped with a KEVEX energy dispersive X-ray spectrometer, revealed crystals with the mean composition $Ba_{1.8}Zn_{2.5}F_{7.4}Cl$ (as obtained by investigations of eight crystals), in agreement with the formulation $Ba_2Zn_2F_7Cl$ deduced from X-ray structure determination.

We also synthesized $Ba_2Co_2F_7Cl$ and $Ba_2Ni_2F_7Cl$ using a chloride flux composed of NaCl + $CoCl_2$ (or $NiCl_2$), allowing the melting points to be lowered. But these preparations gave very bad results as far as the quality of the crystals were concerned, so that they were unusable for X-ray analysis on single crystals. However, single crystals of $Ba_2Co_2F_7Cl$ were isolated by mechanical fragmentation, from a well-crystallized sample obtained in the solid state after heat treatment (2 days at 680°C) and slow cooling (5°C/hr).

Powder samples of the entire $Ba_2M_2F_7Cl$ and $Ba_2MM'F_7Cl$ series were studied by X-ray analysis on a Philips PW1380 or a Siemens D501 diffractometer (Cu$K\alpha$-graphite back monochromator). The cell parameters, refined by a profile matching procedure (11), are reported in Table 1. The evolution of the cell volumes is in full agreement with crystal field theory applied to high spin cations (see Fig. 1).

The melting points of the $Ba_2M_2F_7Cl$ series, measured by a thermal study on DTA Netzsch 404S equipment (heating rate 300°C/hr), are reported in Table 1.

Susceptibility and magnetic measurements were performed in the temperature range 4.2–300 K using a Faraday method ($6.6 < H < 11.2$ T) and a vibrating sample magnetometer, respectively.

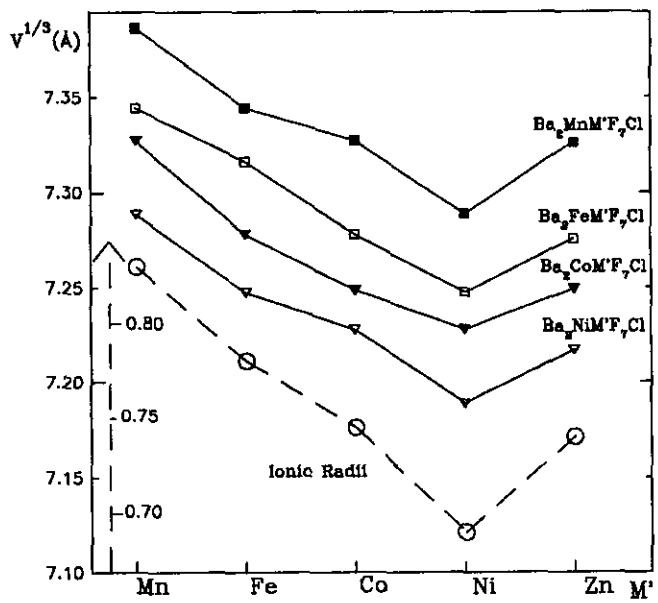

FIG. 1. Evolution of the cell volumes of the $Ba_2MM'F_7Cl$ series as a function of the metallic cations.

X-RAY DATA COLLECTION AND CHARACTERIZATION OF $Ba_2M_2F_7Cl$ (M = Zn, Co)

During preliminary studies on $Ba_2Zn_2F_7Cl$, many crystals selected by optical examination showed systematically double spots on Laue photographs, before a very small and apparently correct one was chosen. Laue and Buerger photographs led to an orthorhombic cell (a =

TABLE 1
Cell Parameters[a] (Å) and Melting Points of the $Ba_2MM'F_7Cl$ Series

	a	b	c	β (°)	V (Å^3)	MP (°C)
$Ba_2Mn_2F_7Cl$	7.941(1)	5.886(1)	8.993(1)	106.52(1)	403.0(2)	615(5), 667(5)[b]
$Ba_2Fe_2F_7Cl$	7.830(1)	5.800(1)	9.003(1)	106.71(2)	391.6(3)	702(5)
$Ba_2Co_2F_7Cl$	7.695(1)	5.787(1)	8.940(1)	106.92(1)	380.9(2)	766(5)
$Ba_2Ni_2F_7Cl$	7.625(1)	5.778(1)	8.806(1)	106.73(1)	371.5(2)	798(5), 852(5)[b]
$Ba_2Zn_2F_7Cl$	7.692(1)	5.795(1)	8.937(1)	106.90(1)	381.2(2)	625(5)
Ba_2MnFeF_7Cl	7.878(1)	5.838(1)	8.988(1)	106.55(1)	396.2(2)	
Ba_2MnCoF_7Cl	7.825(1)	5.844(1)	8.979(1)	106.62(1)	393.4(2)	
Ba_2MnNiF_7Cl	7.766(3)	5.844(1)	8.932(4)	106.64(1)	388.4(2)	
Ba_2MnZnF_7Cl	7.823(1)	5.847(1)	8.969(1)	106.59(1)	393.2(2)	
Ba_2FeCoF_7Cl	7.751(1)	5.796(1)	8.966(1)	106.85(1)	385.5(2)	
Ba_2FeNiF_7Cl	7.700(1)	5.797(1)	8.912(1)	106.85(1)	380.7(2)	
Ba_2FeZnF_7Cl	7.743(1)	5.798(1)	8.960(1)	106.78(1)	385.1(2)	
Ba_2CoNiF_7Cl	7.667(1)	5.789(1)	8.887(1)	106.79(1)	377.6(2)	
Ba_2CoZnF_7Cl	7.695(1)	5.791(1)	8.937(1)	106.92(1)	381.0(2)	
Ba_2NiZnF_7Cl	7.653(1)	5.783(1)	8.873(1)	106.82(1)	375.9(2)	

[a] From powder data (T = 22 ± 2°C).
[b] Two peaks are observed (the last one corresponds to the melting point).

TABLE 2
Crystal Data and Conditions of Data Collection and Refinement for $Ba_2Zn_2F_7Cl$ and $Ba_2Co_2F_7Cl$

	$Ba_2Zn_2F_7Cl$	$Ba_2Co_2F_7Cl$
⟨Data collection (T = 20°C)⟩		
Symmetry	Monoclinic	Monoclinic
Parameters		
a	15.399(4) Å	7.692(3) Å
b	5.801(2) Å	5.783(2) Å
c	8.939(2) Å	8.945(2) Å
β	106.85(2)	106.88(2)°
Calculated density (g cm^{-3})	4.99(1)	4.85(1)
Observed density (g cm^{-3})		4.88(1)
Crystal size	8.2×10^{-5} mm^3	8.7×10^{-5} mm^3
Faces	±(1, 0, 0/0, 1, 0/1, 0, 0)	
Scan mode	$\omega - \Theta$ ($37 \leq N \leq 42$)[a]	$\omega/\Theta = 1 + 0.35\text{tg}\Theta$
Aperture	3 × 3 mm^2	2.5 + 1.5tgΘ (°)
Data collection range	$2\Theta \leq 60°$	$2\Theta \leq 70°$
Standard reflections	−2, 3, 2/8, 0, 2/2, 2, −4	2, −1, 0/0, −2, 0/−2, −1, 0
Measured reflections	2832	3638
Max h, k, l	21, 8, 12	12, 9, 14
Absorption	μ = 169.9 cm^{-1}	μ = 148.7 cm^{-1}
Transmission factors: T_{max}, T_{min}	0.676, 0.495	0.998, 0.770
⟨Refinement conditions⟩		
Program of refinement	SHELX-86	SHELXL-93
Space group	$P2_1/m$ (11)	$P2_1/m$
Parameters	$a/2$ = 7.700(2), b, c, β	
Volume	382.1(4) Å^3	380.8(8) Å^3
Z	2	2
Number of reflections	1122	1905
R(from $2/m$ averaging)	0.035	0.032
Independent reflections	835 ($I > 3\sigma(I)$)	1066 ($I > 2\sigma(I)$)
Number of reflections used in the refinement	795	1065
Number of refined parameters	65	64
Secondary extinction factor	$\varepsilon = 1.9(3)\ 10^{-7}$	none
Max height in the final difference Fourier map	1.9 e · Å^{-3}	1.6 e · Å^{-3}
Reliability factors R; R_w/R_1; wR_2	R = 0.028; R_w = 0.032	R_1[b] = 0.036; wR_2[c] = 0.044
Weighting scheme	$w = 1.03/(\sigma^2(F) + 0.00047F^2)$	$w^d = 1/\sigma^2 I_o + (0.0053\ P)^2$

[a] N steps of $\Delta\omega$ = 0.035,
[b] $R_1 = \sum \| |F_o| - |F_c| \| / \sum |F_o|$.
[c] $wR_2 = (\sum w(I_o - I_c)^2 / \sum wI_o^2)^{1/2}$.
[d] With $P = (I_o + 2I_c)/3$.

29.35 Å, b = 5.78 Å, c = 8.90 Å) with a C Bravais lattice. A random reflection search on a SIEMENS AED2 four-circle diffractometer (Mo$K\alpha$) first confirmed this cell. However, a careful examination of the intensities of equivalent reflections only showed a $2/m$ symmetry instead of the expected *mmm* symmetry for an orthorhombic Laue group. Indeed, a monoclinic P cell was determined after the indexation of the reflections of a long exposure oscillation photograph. The resulting monoclinic cell parameters, refined by a double list procedure from 32 reflections distributed near $2\Theta \approx 30°$—a_m = 15.399(4) Å, b_m = 5.801(2) Å, c_m = 8.939(2) Å, β = 106.85(2)°—are derived from the orthorhombic parameters (a_o, b_o, c_o) by the relation $a_m = a_o/2 \cos(\beta - \pi/2)$, $b_m = b_o$, $c_m = c_o$. The intensity measurement was carried out under the conditions reported in Table 2.

Two conditions limiting possible reflections were observed. The first one—$hk0 : h = 2n$—is not consistent with a monoclinic P lattice (with unique axis b). So we had to discard this pseudo-condition for the space group determination. The second one—$0k0 : k = 2n$—agrees with the $P2_1/m$ space group (or $P2_1$ subgroup). In fact, 010, 030, and 050 reflections were observed, but their Ψ scan analysis ($\Delta\Psi$ = 5°) showed that they were due to a Renninger effect. Calculations were performed using the SHELX-76 (12) and SHELXS-86 (13) programs. Intensities were corrected for Lorentz and polarization effects as well as for absorption.

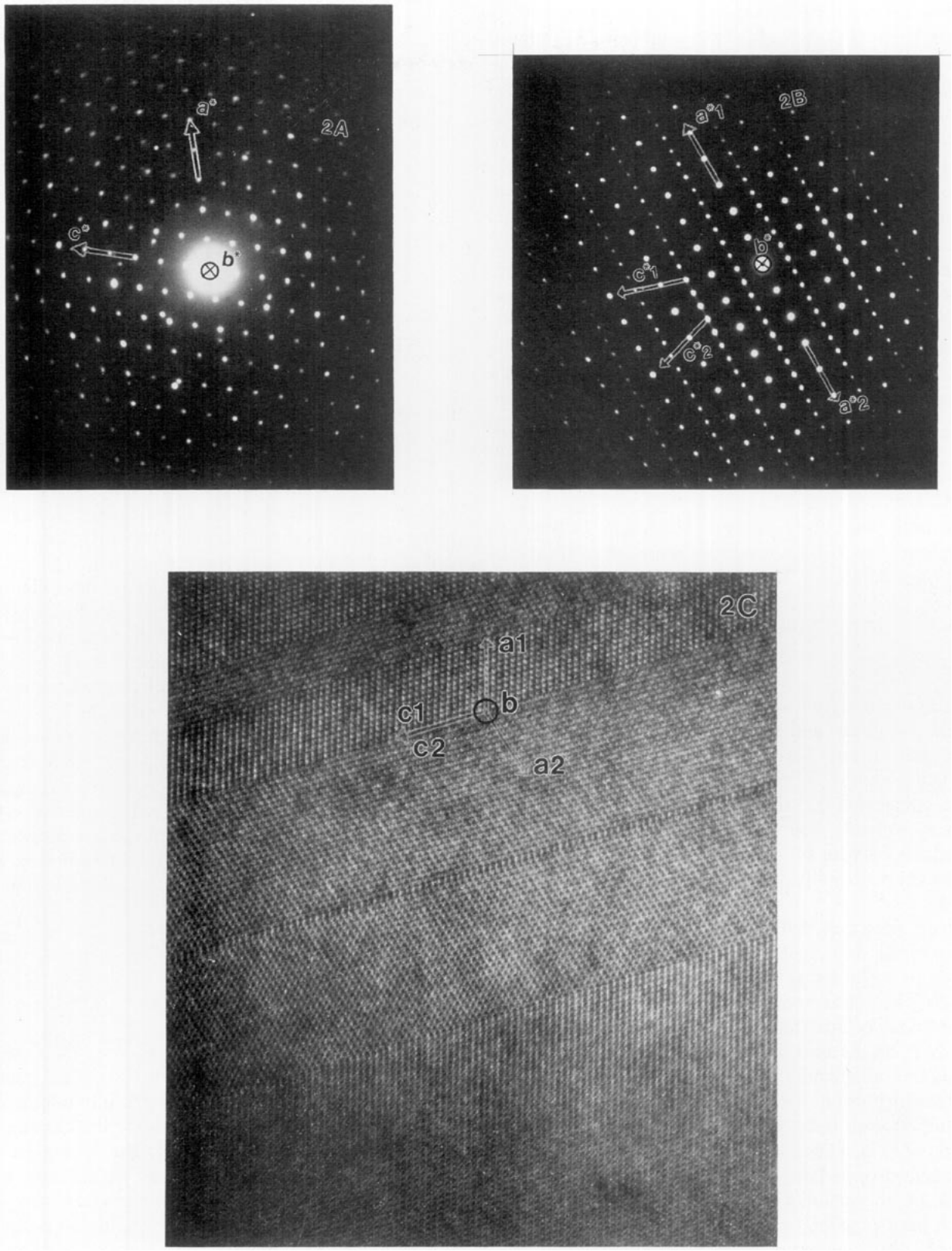

FIG. 2. Selected area electrons diffraction patterns along [0 1 0] zone axis, on an (a) untwinned, (b) twinned part of the observed crystallite. (c) the corresponding HRTEM image.

A single crystal of $Ba_2Co_2F_7Cl$ was examined by the Buerger precession technique, to establish its symmetry and suitability for intensity data collection. This study also led to a monoclinic symmetry and to the $P2_1/m$ space group (or subgroup). It appeared clearly that the single crystal used was not twinned. However, an electron microscopy study performed on powder samples with a JEOL 2000FX electron microscope showed that the main part of the observed crystallites were twinned in the same way as for $Ba_2Zn_2F_7Cl$ (see next paragraph and Fig. 2).

Intensity data for the structure determination were collected on an automated four-circle diffractometer (Enraf-Nonius CAD4) with graphite monochromatized (Mo$K\alpha$) radiation, a scintillation counter, and a pulse-height discriminator. Intensities were corrected for Lorentz and polarization effects, and an empirical absorption correction was made on the basis of psi-scan data. The intensity collection was carried out with the conditions reported in Table 2. Calculations were performed using SHELXL-93 (14).

For both structures, atomic scattering factors and anomalous dispersion corrections were taken from "International Tables for X-ray Crystallography" (15).

STRUCTURE DETERMINATION

(*a*) $Ba_2Zn_2F_7Cl$[3]

Our first attempts to determine the structure with the help of the direct and the heavy atom methods in the $P2_1/m$ space group were all unsuccessful. However, the observed pseudo-condition, limiting the $hk0$ reflections to h even, suggested that the a parameter of the monoclinic cell was probably doubled. Then we supposed that all the reflections with $h = 2n + 1$ originated in a twinning phenomenon (despite the apparent good quality of the crystal).

Indeed, for a new cell parameter $a = a_m/2 = 7.6977$ Å, the use of the option TREF of the SHELXS-86 program allowed us to locate at first one barium and one zinc in 2*e* sites. The refinement of their atomic coordinates led to $R = 0.38$. The analysis of successive difference Fourier maps gave us the position of two other cations (Ba_2 and Zn_2), in the same kind of site ($R = 0.17$). Then we located the chlorine atom in a 2*e* site, three fluorines in 4*f* sites, and one fluorine in a 2*e* site. This led to a $Ba_2Zn_2F_7Cl$ formula ($Z = 2$). The reliability value of the corresponding refinement dropped only to $R = 0.065$, with inconsistent anisotropic thermal motions applied to the barium atoms. Such a poor R value is typical for twinned crystals, because the observed intensity of any reflection is generally the sum of the superimposed intensities from at least two domains.

[3] The lists of structure factors may be obtained upon request from the authors.

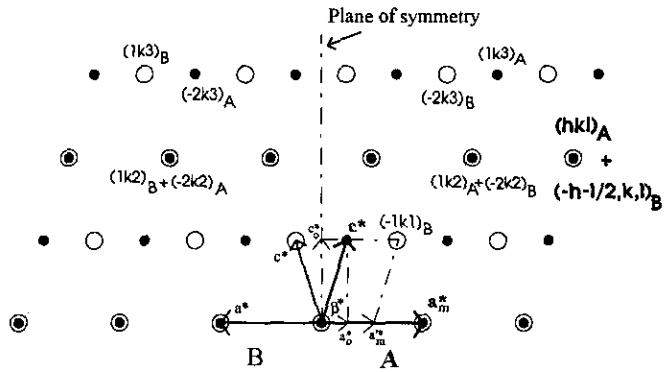

FIG. 3. Reciprocal network of two twinned domains viewed along b^*. Filled and open circles respectively correspond to A and B reciprocal points.

In our case, it can be explained by a twinning process involving two crystal domains, A and B (see the reciprocal network schematized in Fig. 3). Indeed the (bc) symmetry plane of the orthorhombic cell (from which the monoclinic cell is deduced) is the twinning plane which generates the growth of the two components. Thus, the reflections of the second crystal B (open circles) are responsible for the doubling of the a parameter (for example, $(-1k1)_B$, $(-2k3)_B$, $(1k3)_B$), or for the modification of the intensity values of the first crystal A (filled circles) when they superimpose (for example, $(1k2)_A + (-2k2)_B$).

Based on this explanation, we have estimated the relative proportion of the two crystals as $r = 3.5$, from a set of unique hkl reflections with l odd (for example, $r = I_{(1k3)A}/I_{(1k3)B}$). Then, the unique reflections belonging to the crystal B were suppressed in the list of intensities. Finally, the intensities $I_{(h,k,l)}$ of the predominant crystal A, with l even, were corrected using the relations

$$I_{(h,k,l)} = I_{(h,k,l)A} + I_{(\bar{h}-l/2,k,l)B} \quad I_{(h,k,l)A} = rI_{(h,k,l)B},$$

thus

$$I_{(h,k,l)A} = \left[I_{(h,k,l)} - \frac{1}{r} I_{(\bar{h}-l/2,k,l)}\right] \frac{r^2}{r^2-1} \quad \text{with } r = 3.5.$$

The structural refinement of the resulting intensity set, with anisotropic thermal motions for the cations, led to $R = 0.036$. Then the reliability factor decreased to $R = 0.027$ ($R_w = 0.032$) for the last calculation using a weighting scheme and anisotropic thermal motions for all atoms. The twinning hypothesis was then confirmed by this satisfying refinement.

The final positions and thermal parameters are reported in Table 3, whereas Table 4a gives the main interatomic distances and angles.

TABLE 3
Atomic Parameters, Anisotropic Temperature Factors[a] $U_{ij} \times 10^4$ and B_{eq} (Å^2) for $Ba_2Zn_2F_7Cl$ and $Ba_2Co_2F_7Cl$

Atom	site	x	y	z	U_{11}	U_{22}	U_{33}	U_{23}	U_{13}	U_{12}	B_{eq}
Ba_1	2e	0.3317(1)	1/4	0.5871(1)	114(3)	84(3)	91(3)	0	29(2)	0	0.76(3)
Ba_1	*2e*	*0.3303(1)*	*1/4*	*0.5872(1)*	*115(3)*	*99(4)*	*86(3)*	*0*	*36(2)*	*0*	*0.78(1)*
Ba_2	2e	0.3047(1)	1/4	0.0750(1)	139(3)	91(3)	76(3)	0	24(2)	0	0.82(3)
Ba_2	*2e*	*0.3024(1)*	*1/4*	*0.0742(1)*	*128(3)*	*94(4)*	*86(3)*	*0*	*29(2)*	*0*	*0.81(1)*
Zn_1	2e	0.8274(2)	1/4	0.7354(1)	72(5)	83(6)	108(6)	0	7(4)	0	0.72(5)
Co_1	*2e*	*0.8261(2)*	*1/4*	*0.7339(1)*	*82(5)*	*90(6)*	*94(5)*	*0*	*31(5)*	*0*	*0.69(2)*
Zn_2	2e	0.8184(2)	1/4	0.1732(1)	78(5)	79(6)	125(6)	0	26(4)	0	0.75(5)
Co_2	*2e*	*0.8181(2)*	*1/4*	*0.1746(1)*	*92(5)*	*77(6)*	*87(5)*	*0*	*33(5)*	*0*	*0.66(2)*
Cl	2e	0.8825(3)	1/4	0.4701(3)	164(10)	126(12)	145(11)	0	52(9)	0	1.13(11)
Cl	*2e*	*0.8817(3)*	*1/4*	*0.4693(3)*	*186(10)*	*120(10)*	*119(9)*	*0*	*60(8)*	*0*	*1.09(3)*
F_1	4f	0.6302(6)	0.0072(9)	0.1608(5)	179(20)	137(25)	148(22)	−25(18)	57(16)	−17(18)	1.21(21)
F1	*4f*	*0.6300(5)*	*0.0061(10)*	*0.1604(4)*	*194(19)*	*147(26)*	*120(16)*	*24(18)*	*37(15)*	*−50(19)*	*1.23(7)*
F_2	4f	0.0052(8)	0.0002(12)	0.8274(6)	328(26)	375(36)	216(26)	44(24)	79(21)	269(27)	2.42(28)
F2	*4f*	*0.0046(5)*	*0.0013(9)*	*0.8279(4)*	*258(21)*	*386(29)*	*184(17)*	*57(20)*	*56(16)*	*259(23)*	*2.19(8)*
F_3	4f	0.6397(6)	0.0028(9)	0.6552(5)	152(19)	117(24)	116(21)	−43(17)	40(15)	−58(17)	1.01(20)
F3	*4f*	*0.6380(4)*	*0.0037(10)*	*0.6544(4)*	*134(18)*	*113(24)*	*135(17)*	*−39(16)*	*55(15)*	*−23(17)*	*0.98(7)*
F_4	2e	0.7473(9)	1/4	0.9346(8)	213(32)	143(33)	189(33)	0	131(27)	0	1.31(32)
F4	*2e*	*0.7465(7)*	*1/4*	*0.9341(6)*	*93(25)*	*251(32)*	*97(23)*	*0*	*38(21)*	*0*	*1.14(9)*

Note. Standard deviations are given in parentheses. $Ba_2Co_2F_7Cl$ printed in italics.

[a] The vibrational coefficient relate to the expression: $T = \exp[-2\pi^2(h^2a^{*2}U_{11} + k^2b^{*2}U_{22} + l^2c^{*2}U_{33} + 2hka^*b^*U_{12} + 2hla^{**}c^*U_{13} + 2klb^*c^*U_{23})]$.

(*b*) *$Ba_2Co_2F_7Cl$*[4]

The structure of $Ba_2Co_2F_7Cl$ was determined by interpretation of the Patterson map, which resulted in the positions of the barium and cobalt atoms. Those of the chlorine and fluorine atoms were located in subsequent difference Fourier maps. The final conventional R (based on F_o) and wR_2 (based on F_o^2), including anisotropic thermal motions for all atoms, are respectively 0.036 and 0.044 for 1065 reflections and 64 refined parameters. The atomic and thermal parameters are listed in Table 3 and the main interatomic distances in Table 4b.

Interpretation of electron diffraction patterns led to the same twinning explanation as for the $Ba_2Zn_2F_7Cl$ single crystal. We can see for example in Fig. 2 that the [1 0 0]* direction is a symmetry axis for the [0 1 0] zone axis diffraction pattern. This corresponds obviously to the (1 0 0) symmetry plane introduced by the twinning phenomenon, which is directly revealed by HRTEM images.

It must be noted that we have checked the $P2_1$ noncentrosymmetrical space group for each set of data (with 43 additional refined parameters). Although slightly better reliabilities were obtained, this solution had to be rejected, from Hamilton tests. On the other hand, the nonlinear optical measurements, performed on a set of powder specimens of the series, did not show any indication of agreement with a noncentrosymmetrical space group.

[4] The lists of structure factors may be obtained upon request from the authors.

POWDER DATA REFINEMENT ON THE $Ba_2MM'F_7Cl$ SERIES

The M^{2+} transition cations have close diffusion factors, as far as X-ray diffraction is concerned. Therefore, it is difficult to discern between two sites occupied by different transition cations using an X-ray study based on the reliability values of a Rietveld structure refinement. However, if the two cations have different ionic radii, the cationic ordering can be judged by the criterion of interatomic distances. We then decided to study the Ba_2MnNiF_7Cl compound, where the largest and smallest ionic radii of the 3*d* transition metals series (Mn^{2+} = 0.83 Å and Ni^{2+} = 0.69 Å) are associated. This compound was heated at 600°C for 12 hr, and then slowly cooled to room temperature (10°C/hr).

X-ray powder data collection was performed on a SIEMENS D501 diffractometer, with back-monochromatized

TABLE 4a
Main Interatomic Distances (Å) and Angles (°) with esd in $Ba_2Zn_2F_7Cl$

Ba_1 Polyhedron [6 + 3] (m)			Ba_2 Polyhedron [12] (m)		
2x	$Ba–F_1$	2.647(5)	2x	$Ba–F_1$	2.745(7)
2x	$Ba–F_3$	2.677(5)	2x	$Ba–F_3$	2.748(7)
2x	$Ba–F_3$	2.685(5)	2x	$Ba–F_1$	2.782(4)
2x	Ba–Cl	3.302(1)	2x	$Ba–F_4$	2.926(4)
1x	Ba–Cl	3.310(2)	2x	$Ba–F_2$	3.061(4)
			2x	$Ba–F_2$	3.125(8)
$\langle Ba_1–F\rangle$ = 2.67 Å			$\langle Ba_2–F\rangle$ = 2.90 Å		
$\langle Ba_1–Cl\rangle$ = 3.30 Å			$d_{Shannon}$ = 2.92 Å		
$\langle Ba_1–F, Cl\rangle$ = 2.88 Å					

Zn_1 Octahedron (m)

Zn_1	F_2	F_2	F_3	F_3	F_4	Cl
F_2	**1.999(8)**	2.899(9)	4.011(6)	2.788(6)	2.841(6)	3.382(5)
F_2	93.0(0.5)	**1.999(5)**	2.788(6)	4.011(6)	2.841(6)	3.382(5)
F_3	175.8(0.4)	88.0(0.5)	**2.015(6)**	2.868(7)	2.789(7)	3.176(3)
F_3	88.0(0.5)	175.8(0.4)	90.7(0.4)	**2.015(4)**	2.789(7)	3.176(3)
F_4	89.2(0.5)	89.2(0.5)	86.8(0.5)	86.8(0.5)	**2.046(7)**	4.564(6)
Cl	96.0(0.3)	96.0(0.3)	88.0(0.3)	88.0(0.3)	172.5(0.3)	**2.527(3)**

$\langle Zn_1–F, Cl\rangle$ = 2.10 Å; $d_{Shannon}$ $Zn_1–F$ = 2.05 Å
$d_{Shannon}$ Zn–F,Cl = 2.13 Å; $d_{Shannon}$ $Zn_1–Cl$ = 2.55 Å

Zn_2 Octahedron (m)

Zn_2	F_2	F_2	F_1	F_1	F_4	Cl
F_2	**1.989(7)**	2.902(9)	2.779(7)	3.987(10)	2.814(7)	3.354(4)
F_2	93.7(0.6)	**1.989(8)**	3.987(10)	2.779(7)	2.814(7)	3.354(4)
F_1	88.3(0.5)	176.3(0.6)	**2.000(6)**	2.816(7)	2.818(6)	3.207(4)
F_1	176.3(0.6)	88.3(0.5)	89.5(0.4)	**2.000(5)**	2.818(6)	3.207(4)
F_4	88.5(0.5)	88.5(0.5)	88.4(0.5)	88.4(0.5)	**2.042(6)**	4.594(7)
Cl	94.3(0.3)	94.3(0.3)	88.6(0.3)	88.6(0.3)	175.8(0.4)	**2.555(2)**

$\langle Zn_2–F, Cl\rangle$ = 2.10 Å

Cu$K\alpha$. The method of filling the sample holder, described in Ref. (16), was used to avoid possible preferential orientation. The conditions of recording and refinement are reported in Table 5. The structure refinement by a modified Rietveld method, called ARIT4 (17), with anisotropic B factors for barium and isotropic B values for Mn, Ni, Cl, and F, led to the conventional Rietveld reliability factors R_i = 5.14%, R_p = 9.14%, and R_{wp} = 10.78% (see Fig. 4). Similar R values were obtained by an inversion of the Mn^{2+} and Ni^{2+} positions, as well as by their statistical repartition. Tables 6a and 6b give the final atomic positions and the selected interatomic distances, respectively. In the three cases, the mean M–(F, Cl) distances (called here after M–X), M_1–X = 2.17 Å, and M_2–X = 2.08 Å, remain unchanged. They are in good agreement with the expected Shannon values for M_1 = Mn and M_2 = Ni(Mn–X = 2.22 Å and Ni–X = 2.08 Å). This showed that the two cations are probably ordered on the 2e cationic sites. The atomic coordinates for Mn and Ni are respectively x = 0.8331(5), y = 1/4, z = 0.7358(6), and x = 0.8136(6), y = 1/4, z = 0.1785(8).

A partial cationic disorder might appear for the other combined compounds having cations with close ionic radii (Fe–Ni, Co–Ni, Zn–Co series . . .), even after slow cooling. Nevertheless, the study of the magnetic properties of these phases seem to be of interest.

DESCRIPTION OF THE STRUCTURE

The $Ba_2M_2F_7Cl$ structure can be described as mainly built up from $[MX_6]^{4-}$ octahedra which share vertices, giving rise to puckered $[MX_4]^{2-}$ layers, between which the large Ba^{2+} cations are inserted (Fig. 5a). The octahedra are *trans*-connected in the c direction and *cis*-connected in the b direction. Such a connection mode is observed in the orthorhombic $BaZnF_4$ structure type (19) (a = 4.206 Å, b = 14.563 Å, c = 5.841 Å) and in $NaCrF_4$ (20) (a = 7.862 Å, b = 5.328 Å, c = 7.406 Å, β = 101.65°), which adopts the monoclinic $NaNbO_2F_2$ (21) structure type (Figs. 5b and 5c, respectively). Nevertheless, in the latter structures, the octahedra are rotated around a pseudo-axis defined by the fluorine atoms in *trans* position, whereas in the title compounds the octahedra mainly appear as tilted in the (ac) plane. This difference is obviously related to the presence of chlorine atoms in the coordination number of the metallic cations. Indeed, the $[MF_5Cl]^{4-}$ octahedra

TABLE 4b
Main Interatomic Distances (Å) and Angles (°) with esd in $Ba_2Co_2F_7Cl$

Ba_1 *Polyhedron [6 + 3] (m)*			Ba_2 *Polyhedron [12] (m)*		
2x	$Ba–F_1$	2.645(4)	2x	$Ba–F_1$	2.741(4)
2x	$Ba–F_3$	2.680(4)	2x	$Ba–F_3$	2.761(4)
2x	$Ba–F_3$	2.683(4)	2x	$Ba–F_1$	2.797(4)
2x	Ba–Cl	3.290(2)	2x	$Ba–F_4$	2.918(1)
1x	Ba–Cl	3.305(3)	2x	$Ba–F_2$	3.041(4)
			2x	$Ba–F_2$	3.111(4)
$\langle Ba_1–F\rangle$ = 2.67 Å			$\langle Ba_2–F\rangle$ = 2.89 Å		
$\langle Ba_1–Cl\rangle$ = 3.30 Å			$d_{Shannon}$ = 2.92 Å		
$\langle Ba_1–F, Cl\rangle$ = 2.88 Å					

Co_1 Octahedron (m)

Co_1	F_2	F_2	F_3	F_3	F_4	Cl
F_2	**2.000(4)**	2.881(7)	4.006(6)	2.799(6)	2.833(6)	3.392(5)
F_2	93.4(0.3)	**2.000(4)**	2.799(6)	4.006(6)	2.833(6)	3.392(5)
F_3	175.2(0.2)	88.5(0.2)	**2.010(5)**	2.852(7)	2.790(7)	3.179(4)
F_3	88.5(0.2)	175.2(0.2)	90.4(0.3)	**2.010(5)**	2.790(7)	3.179(4)
F_4	88.6(0.2)	88.6(0.2)	86.7(0.2)	86.7(0.2)	**2.055(5)**	4.573(5)
Cl	96.4(0.1)	96.4(0.1)	88.2(0.1)	88.2(0.1)	172.8(0.2)	**2.527(2)**

$\langle Co_1–F, Cl\rangle$ = 2.10 Å — $d_{Shannon}$ $Co_1–F$ = 2.06 Å
$d_{Shannon}$ Co–F,Cl = 2.14 Å — $d_{Shannon}$ $Co_1–Cl$ = 2.56 Å

Co_2 Octahedron (m)

Co_2	F_2	F_2	F_1	F_1	F_4	Cl
F_2	**2.000(4)**	2.910(7)	2.785(7)	3.997(7)	2.820(7)	3.363(5)
F_2	93.4(0.3)	**2.000(4)**	3.997(7)	2.785(7)	2.820(7)	3.363(5)
F_1	88.3(0.2)	175.6(0.2)	**2.000(5)**	2.824(6)	2.821(6)	3.206(4)
F_1	175.6(0.2)	88.3(0.2)	89.8(0.3)	**2.000(5)**	2.821(6)	3.206(4)
F_4	88.0(0.1)	88.0(0.1)	88.0(0.1)	88.0(0.1)	**2.061(5)**	4.596(4)
Cl	94.9(0.1)	94.9(0.1)	89.1(0.1)	89.1(0.1)	175.8(0.2)	**2.539(2)**

$\langle Co_1–F, Cl\rangle$ = 2.10 Å

TABLE 5
Conditions of Powder Data Recording (300 K) and Refinement for Ba_2MnNiF_7Cl

Space group	$P2_1/m$			
2Θ range (°)	7–130			
Step scan (°2Θ)	0.02			
Time/Step (sec)	37			
Receiving slit (°)	0.15			
Number of reflections	1493			
Number of parameters	46			
Zero point: (°2Θ)	−0.039			
Program used	ARIT4[a]			
Background	Selected by hand			
Profile parameters[b,c]	U_1 = 0.067(7)	V_1 = −0.06(1)	W_1 = 0.069(2)	
for a = 120, l = 59	U_2 = −0.16(4)	V_2 = 0.33(6)	W_2 = 1.32(2)	
	C = −0.046(1)	D = −0.074(3)		
Reliability factors	R_i = 5.39%	R_p = 9.14%	R_{wp} = 10.78%	R_{exp} = 3.14%

[a] *a* modified Rietveld method which describes the line profile by means of Fourier coefficients.
[b] U_1, V_1, W_1: parameters related to the width of the reflections (same meaning as in the formulation of Caglioti (18)).
U_2, V_2, W_2: parameters related to the shape of the reflections.
a: number of step scan intervals defining the width of the reflections.
l: number of Fourier coefficients.
C, D: parameters related to the asymmetry of the reflections.
[c] For more information see Ref. 11.

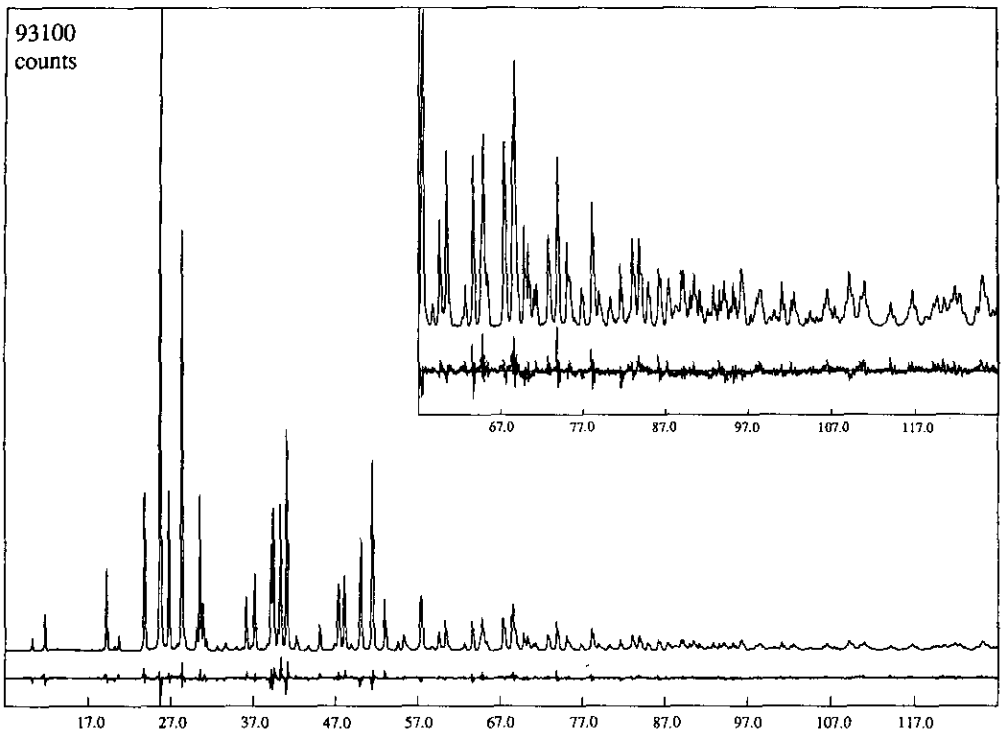

FIG. 4. Calculated X-ray intensities vs 2Θ (°) of Ba_2MnNiF_7Cl. The difference pattern ($I_{obs} - I_{calc}$) appears below, at the same scale (inset magnified by 6).

TABLE 6a
Atomic Parameters, Anisotropic Temperature Factors $\beta_{ij} \times 10^4$ and B ($Å^2$)[a] for Ba_2MnNiF_7Cl

Atom	site	x	y	z	β_{11}	β_{22}	β_{33}	β_{23}	β_{13}	β_{12}	B
Ba_1	2*e*	0.3285(2)	1/4	0.5851(4)	61(5)	145(9)	13(3)	0	−6(4)	0	1.31(7)
Ba_2	2*e*	0.3134(2)	1/4	0.0769(4)	92(5)	54(8)	26(3)	0	5(4)	0	1.24(6)
Mn	2*e*	0.8331(5)	1/4	0.7358(6)							1.15(11)
Ni	2*e*	0.8136(6)	1/4	0.1785(8)							2.02(12)
Cl	2*e*	0.8818(6)	1/4	0.4706(12)							2.23(11)
F_1	4*f*	0.6405(11)	0.0070(16)	0.1638(20)							2.26(9)
F_2	4*f*	−0.0250(12)	−0.0413(16)	0.8230(7)							2.26(9)
F_3	4*f*	0.6342(11)	−0.0097(16)	0.6571(20)							2.26(9)
F_4	2*e*	0.7467(11)	1/4	0.9432(20)							2.26(9)

Note. One isotropic temperature factor was refined for all F atoms.
[a] The β and B values relate to the expressions: $\exp(-[\beta_{11}h^2 + \beta_{22}k^2 + \beta_{33}l^2 + \beta_{12}hk + \beta_{13}hl + \beta_{23}kl])$ and $\exp(-B[\sin\theta/\lambda]^2)$ respectively.

TABLE 6b
Main Mean Interatomic Distances in Ba_2MnNiF_7Cl

Ba_1 Polyhedron [6 + 3]	Ba_2 Polyhedron [12]
$\langle Ba_1–F\rangle$ = 2.68 Å $\langle Ba_1–Cl\rangle$ = 3.32 Å	
$\langle Ba_1–F, Cl\rangle$ = 2.90 Å	$\langle Ba_2–F\rangle$ = 2.89 Å
Mn^{2+} octahedron	Ni^{2+} octahedron
$\langle Mn–F\rangle$ = 2.11 Å ($d_{Shannon}$: 2.14 Å)	$\langle Ni–F\rangle$ = 2.00 Å ($d_{Shannon}$: 2.00 Å)
$\langle Mn–Cl\rangle$ = 2.50 Å ($d_{Shannon}$: 2.64 Å)	$\langle Ni–Cl\rangle$ = 2.51 Å ($d_{Shannon}$: 2.50 Å)
$\langle Mn–F, Cl\rangle$ = 2.17 Å ($d_{Shannon}$: 2.22 Å)	$\langle Ni–F, Cl\rangle$ = 2.08 Å ($d_{Shannon}$: 2.08 Å)

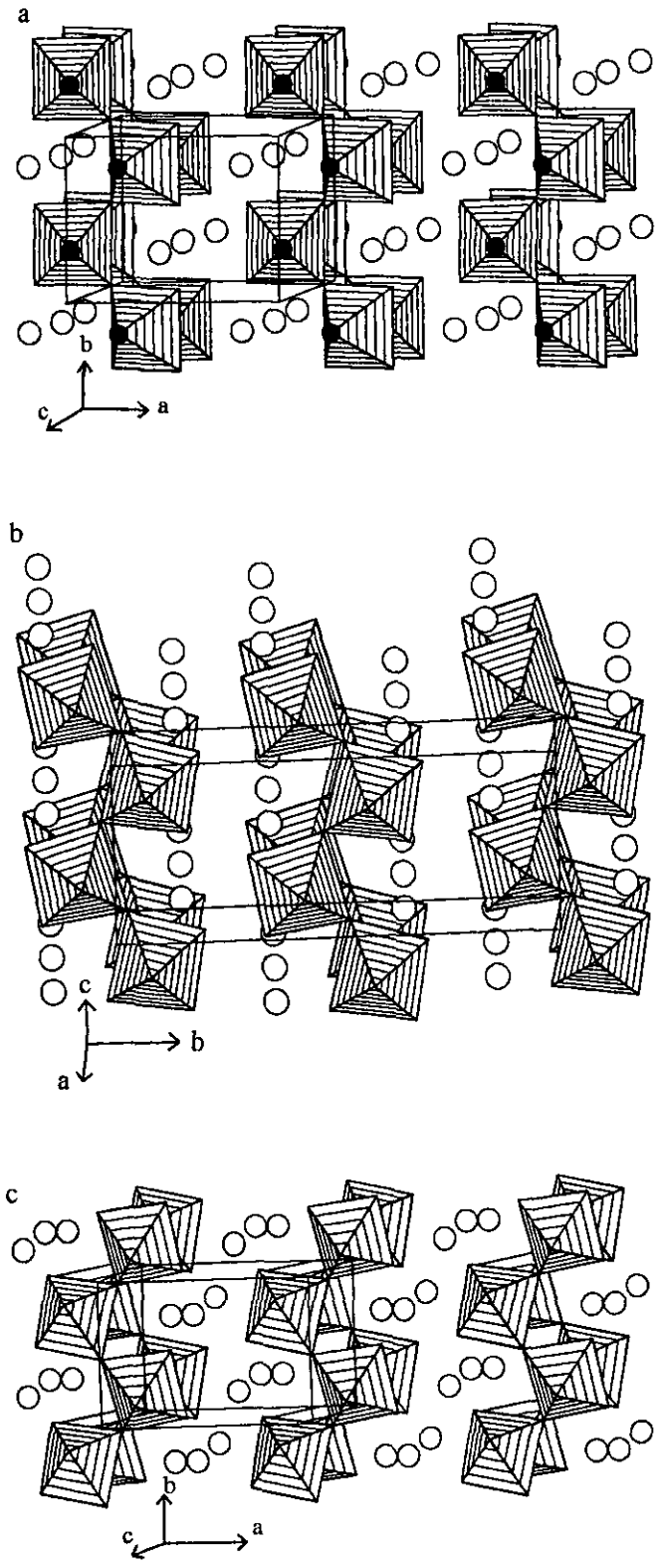

FIG. 5. (a) Perspective view of the puckered layer of octahedra,in the $Ba_2Zn_2F_7Cl$ structure ($P2_1/m$). Filled and open circles correspond to the chlorine and the barium atoms respectively. (b) Perspective view of the $BaZnF_4$ structure ($Cmc2_1$). (c) Perspective view of the $NaCrF_4$ structure ($P2_1/c$).

encountered in the $Ba_2M_2F_7Cl$ compounds are much more distorted than the $[MF_6]^{4-}$ octahedra of the $BaZnF_4$ and $NaCrF_4$ structures. In fact, the square planes of the octahedra are almost regular, with four M–F distances close to 2.00 Å ($1.989 < d < 2.015$ Å and $2.000 < d < 2.010$ Å respectively for M = Zn, Co). The distortion occurs in the axial direction of the polyhedra (c direction), where the mean M–F_4 and M–Cl distances (respectively 2.044, 2.541 Å and 2.058, 2.533 Å) are close to the sum of the ionic radii (2.05, 2.55 Å and 2.06, 2.56 Å). One can notice that the two terminal fluorines (F_1 and F_3) do not exhibit the shortest M–F distances, as usually observed for non-bridging positions.

Figure 6 shows the *trans* connections between octahedra for $Ba_2Zn_2F_7Cl$. A succession of two short (Zn–F) and two long (Zn–Cl) distances is observed in the c direction. This explains the increase in the c parameter (≈8.94 Å) compared to the a parameter of the $BaZnF_4$ structure (2×4.206 Å). The tilting of the octahedra in the (ac) plane is also evidenced: the bridging angles, Zn_1–Cl–Zn_2 and Zn_1–F_4–Zn_2, deviate by 19.9(1)° and 31.6(4)°, respectively, from the ideal 180° value. This tilting mode allows the chlorine and fluorine atoms to move away from the c direction, and consequently allows the Ba_1 and Ba_2 atoms to stay almost lined up, as in the $BaZnF_4$ structure.

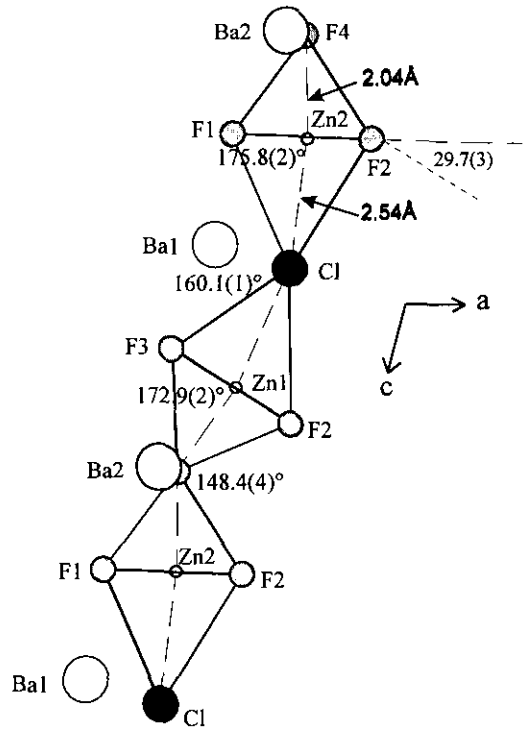

FIG. 6. (010) projection of a $(ZnF_5Cl)^{4-}$ octahedra chain in the $Ba_2Zn_2F_7Cl$ structure (the Zn, Cl, and F_4 atoms are at y = 1/4, the Ba atoms are at y = 3/4).

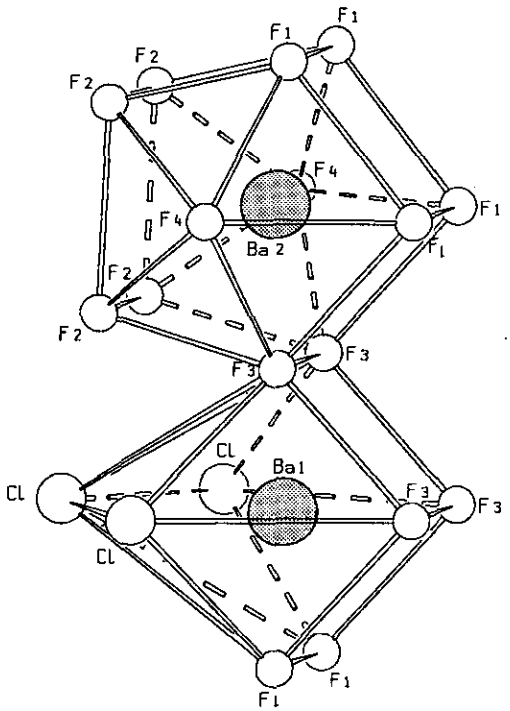

FIG. 7. The two types of barium environment encountered in the $Ba_2M_2F_7Cl$ structures.

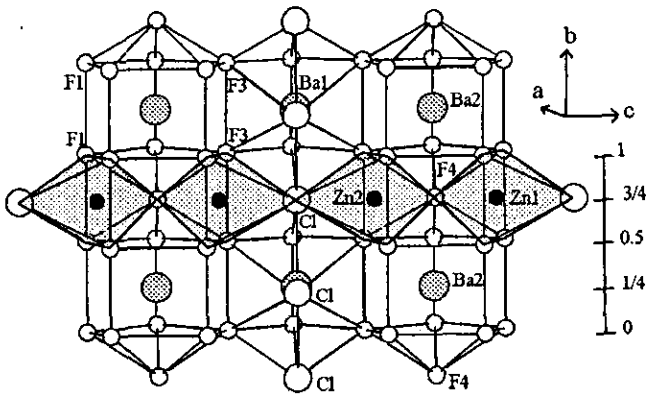

FIG. 8. Perspective view of the (*bc*) planes of polyhedra.

Two kinds of barium polyhedra are encountered in the $Ba_2M_2F_7Cl$ structure. The Ba_1 atom is in a 9-fold coordination (6F + 3Cl), whereas the Ba_2 atom is in a 12-fold coordination (12F). A perspective view is given in Fig. 7. One can remember that a single kind of coordination is found for the $BaZnF_4$ and $NaCrF_4$ structure (11 and 8 respectively). The 12-fold coordinated Ba_2 atom looks like a dicapped pentagonal prism corresponding to the 1–5–5–1 coordination type, as observed in $NaBaZrF_7$ (22). The mean Ba_2–F distance (2.90 Å/2.89 Å) is close to the Shannon expected value (2.92 Å, with *F* in 4-fold coordination). The Ba_1 polyhedron, $(BaF_6Cl_3)^{7-}$, can be seen as a distorted prism with a pentagonal base, leading to a 2–5–2 coordination type. The mean Ba_1–Cl distance (3.30 Å/3.29 Å) is close to the sum of the ionic radii (3.28 Å), but the Ba_1–F distances ($2.65 < d < 2.69$ Å and $2.64 < d < 2.68$ Å) are shorter than the expected value (2.78 Å). This is the first time, to our knowledge, that this kind of (BaF_6Cl_3) polyhedron has been observed. However, 9-fold coordinated (BaF_8Cl) and (BaF_4Cl_5) barium polyhedra have been reported in $Ba_{10}Al_2F_{25}Cl$ (4, 23) and BaFCl (6), respectively. It is noticeable that in these $(BaF_{9-n}Cl_n)$ polyhedra, the mean Ba–Cl distances (3.38/3.30/3.27 Å respectively for $n = 1/3/5$) decrease and get closer to the expected Shannon value (3.28 Å), as *n* increases. Correlatively, the mean Ba–F distances also decrease (2.76/2.67/2.65 Å), but depart from the calculated value (2.78 Å).

Taking into account the barium polyhedra, it is possible to describe the structure as built up from a three-dimensional $[Ba_2F_7Cl]^{4-}$ network. Indeed, in the *b* direction, each polyhedron shares two vertices (2Cl for Ba_1, and $2F_4$ for Ba_2) and two edges (F_3–F_3 and F_1–F_1) with two neighboring polyhedra. Such a connection mode gives rise to (*bc*) planes of polyhedra, as illustrated in Fig. 8 (this figure also displays the MF_5Cl octahedra subnetwork). As similar neighboring planes, moved forward $\frac{1}{2}b$, are observed with respect to the $P2_1/m$ symmetry, a three-dimensional $[Ba_2F_7Cl]^{4-}$ framework is created: the $(Ba_{(2)}F_{12})$ polyhedra of successive planes share F–F edges, and the $(Ba_{(1)}F_6Cl_3)$ polyhedra are linked by both Cl–Cl and F–F edges. Obviously the three-dimensional network of the barium polyhedra can also be thought of as consisting of successive (*ab*) planes, linked together by F–F edges.

MAGNETIC BEHAVIOR

(*a*) *$Ba_2M_2F_7Cl$ Series*

The thermal variations of the reciprocal magnetic susceptibility are shown in Fig. 9. The observed antiferromagnetic behavior is in agreement with the prediction of the Kanamori–Goodenough rules (24, 25), for octahedra sharing vertices (each *M* cation being surrounded by four similar cations). For $Ba_2Ni_2F_7Cl$, a peculiarity appears in the form of a marked cusp at 93 K (observed whatever the method of synthesis of three samples). This cusp probably corresponds to the 3D magnetic order temperature, whereas the 2D magnetic order occurs around 180 K. A comparison with the magnetic results of the $BaMF_4$ series is possible by looking at Table 7. Similar magnetic ordering temperatures are observed. It is well known that for layered structures, the minimum of the inverse suscep-

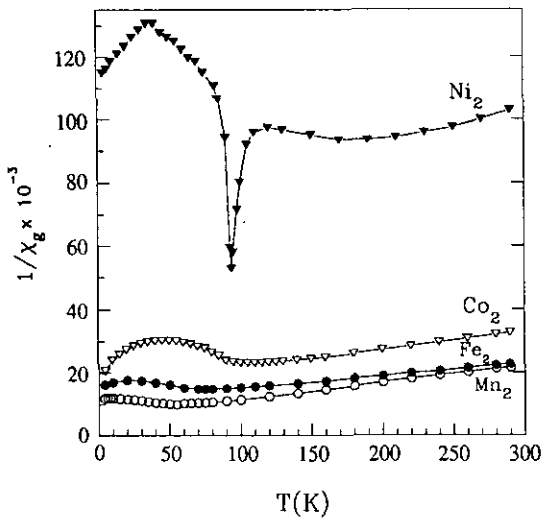

FIG. 9. Magnetic susceptibility curves of the $Ba_2M_2F_7Cl$ family.

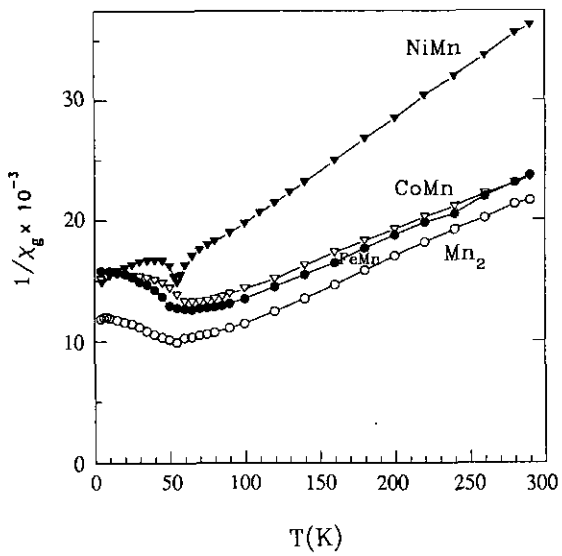

FIG. 10. Magnetic susceptibility curves of the $Ba_2M'MnF_7Cl$ family.

tibility curves at T_{max} does not correspond to the true Néel temperature (26). For the $BaFeF_4$ compound, the discrepancy of the T_{max} and T_N temperatures between susceptibility and Mössbauer measurements is about 25 K. In our chlorofluoride, the same phenomenon is observed.

In a general way, the magnetic behaviors of the $Ba_2M_2F_7Cl$ and $BaMF_4$ series are close to each other, despite some differences in the M–F–M superexchange angles and the M–M distances, as reported in Table 8. Only the calculations of the exchange integrals (M–Cl–M and M–F–M) will provide us with information about the contribution of the chlorine atom in such a two-dimensional structure.

(*b*) *$Ba_2MM'F_7Cl$ Series*

Figures 10 to 14 show the plots of χ_g^{-1} vs T, for the five families of the series. The compounds involving two paramagnetic cations (each M cation being surrounded by four M' cations show macroscopic antiferromagnetic behavior, also in agreement with the Kanamori–Goodenough rules. At 10 K, the measurement of the magnetization vs

TABLE 7
Magnetic Data of the $Ba_2M_2F_7Cl$, $BaMF_4$ and $Ba_2MM'F_7Cl$ Series

$Ba_2M_2F_7Cl$ series		$BaMF_4$ series		
T_{max} (from $1/\chi$)	T_N (Mössbauer)	T_{max} (from χ)	T_N ([a])	T_N (Mössbauer)
$Ba_2Mn_2F_7Cl$ ≈ 57 K		$BaMnF_4$ ≈ 50 K (27)	25 K (27)	
$Ba_2Fe_2F_7Cl$ ≈ 75 K	56 K (28)	$BaFeF_4$ ≈ 75 K (29)		54 K (29)
$Ba_2Co_2F_7Cl$ ≈ 110 K		$BaCoF_4$ ≈ 100 K (30)	70 K (30)	
$Ba_2Ni_2F_7Cl$ ≈ 180 K		$BaNiF_4$ ≈ 150 K (31)	<77 K (31)	

$Ba_2MM'F_7Cl$ series		
T_{max} (from $1/\chi$)	T_N (Mössbauer)	T_N (from $1/\chi$)
Ba_2FeMnF_7Cl ≈ 65 K		Ba_2MnCoF_7Cl ≈ 70 K
Ba_2FeCoF_7Cl ≈ 58 K	59 K (28)	Ba_2MnNiF_7Cl ≈ 55 K
Ba_2FeNiF_7Cl ≈ 78 K	78 K (28)	Ba_2CoNiF_7Cl ≈ 100 K

Note. References are indicated in parentheses.
[a] Determined by other experimental techniques.

TABLE 8
Angles and Distances Related to the Superexchange Interactions for the $BaMF_4$ and the $Ba_2MM'F_7Cl$ Series

$BaMF_4$ series[a]		$Ba_2MM'F_7Cl$ series	
$(M\text{–}F\text{–}M) \approx 167°$	$d_{M\text{–}M} \approx 4.2$ Å	$(M\text{–}F_4\text{–}M) \approx 148°$	$d_{M\text{–}M} \approx 3.9$ Å
		$(M\text{–}Cl\text{–}M) \approx 160°$	$d_{M\text{–}M} \approx 5.0$ Å
$(M\text{–}F\text{–}M) \approx 149°$	$d_{M\text{–}M} \approx 3.9$ Å	$(M\text{–}F_2\text{–}M) \approx 156°$	$d_{M\text{–}M} \approx 3.9$ Å
Interlayers distance	$d_{M\text{–}M} \approx 6.0$ Å	Interlayers distance	$d_{M\text{–}M} \approx 6.0$ Å

[a] From (19).

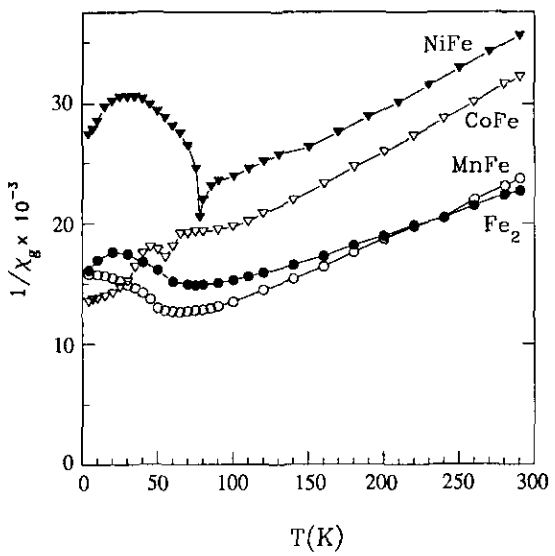

FIG. 11. Magnetic susceptibility curves of the $Ba_2M'FeF_7Cl$ family.

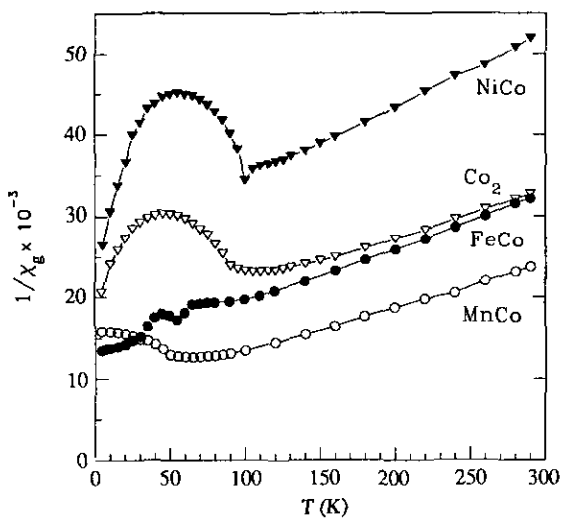

FIG. 12. Magnetic susceptibility curves of the $Ba_2M'CoF_7Cl$ family.

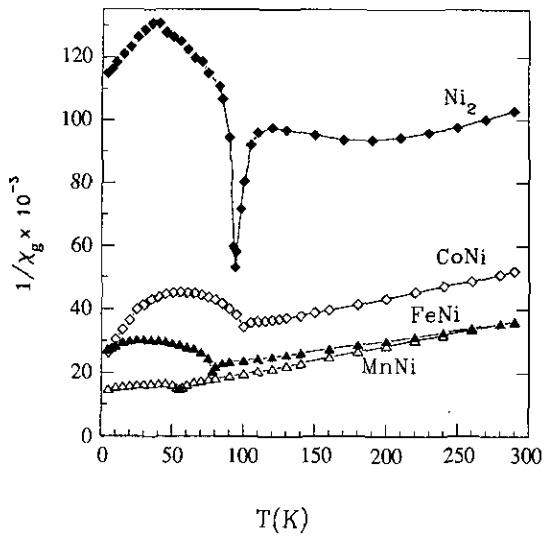

FIG. 13. Magnetic susceptibility curves of the $Ba_2M'NiF_7Cl$ family.

the applied field for Ba_2MnNiF_7Cl shows no ferromagnetic component, and confirms this result. It is noticeable that, for each compound of the $Ba_2M'NiF_7Cl$ family (see Fig. 13), (i) the observed cusps on the $\chi^{-1} = f(T)$ curves correspond to the 3D magnetic order temperature, as proved by the Mössbauer measurement (see Table 7); and (ii) the magnetic order appears within a narrow range of temperature, in comparison with the broad minima observed for the other families, except for the Ba_2FeCoF_7Cl compound (Fig. 12). Concerning the $Ba_2ZnM'F_7Cl$ family, no magnetic transition was observed till 4.2 K. On the supposition that the cations are strictly ordered, the shape of the curves below 50 K (Fig. 14) indicates that the next nearest neighbor interactions are not negligible, and probably are antiferromagnetic.

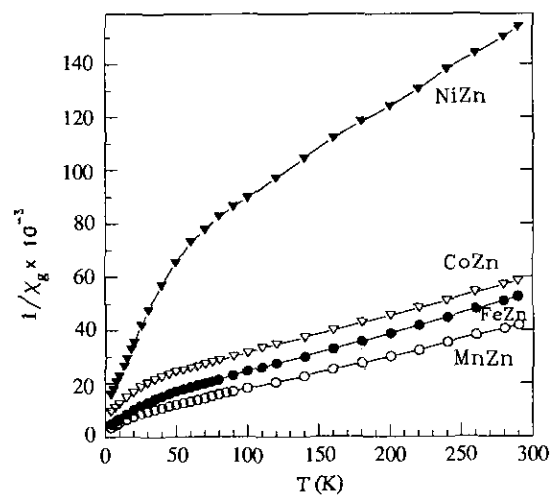

FIG. 14. Magnetic susceptibility curves of the $Ba_2M'ZnF_7Cl$ family.

CONCLUSION

We have synthesized a full series of two-dimensional chlorofluorides. The structure of these $Ba_2MM'F_7Cl$ compounds is related to the $BaZnF_4$ and $NaCrF_4$ structure types. In opposition to $BaZnF_4$, our structure remains centrosymmetrical. The novelty of this structure consists in the presence of (MF_5Cl) octahedra, *cis* connected along the *c* direction, as well as in the existence of two crystallographic sites allowing a cationic order between *M* and *M'*. Consequently, a succession of short and long intercationic distances—3.9 and 5.0 Å—is observed with the sequence (*–M–*F*–M'–*Cl*–M–*), along the [001] direction. Such a situation could have modified the magnetic properties. In fact, the magnetic study showed an antiferromagnetic behavior, as usually observed in the two-dimensional fluorinated compounds. More experimental work should be undertaken in order to estimate the exact contribution of the chlorine atom in the magnetic properties of this series. For this purpose, neutron diffraction is undertaken for $Ba_2Co_2F_7Cl$, $Ba_2Ni_2F_7Cl$, and Ba_2MnNiF_7Cl. Mössbauer study and calculations of the exchange integrals are also in progress.

ACKNOWLEDGMENTS

The authors are grateful to Dr. R. Retoux for X-ray data collection, to Professor M. Leblanc for helpful discussions concerning the twinning phenomenon, to Dr. Y. Laligant for the EDX analysis, and to Dr. J. M. Grenèche for the Mössbauer study in Le Mans. We also thank Dr. J. Durand (University of Montpellier) for optical nonlinear measurements.

REFERENCES

1. D. Babel and A. Tressaud, *in* "Inorganic Solid Fluorides" (P. Haggenmuller, Ed.) p. 77. Academic Press, New York, 1985.
2. G. Bergerhoff and R. Sievers, *Nachr. Dok.* **40,** 27 (1989).
3. J. C. Dewan, A. J. Edwards, and J. J. Guy, *J. Chem. Soc. Dalton Trans.* 2623 (1986).
4. A. Hemon and G. Courbion, *J. Solid State Chem.* **81,** 293 (1989).
5. A. Le Bail, A. Hemon, and G. Courbion, *J. Solid State Chem.* **107,** 234 (1993).
6. M. Sauvage, *Acta Crystallogr. Sect. B* **30,** 2786 (1974).
7. E. Fessenden and S. Z. Lewin, *J. Am. Chem. Soc.* **77,** 4221 (1955).
8. J. Darriet, M. Ducau, M. Feist, and A. Tressaud, *Eur. J. Solid State Inorg. Chem.* **29,** 435 (1992).
9. J. Nouet, C. Jacoboni, G. Ferey, J. Y. Gerard, and R. de Pape, *J. Cryst.Growth* **47,** 699 (1979).
10. G. Courbion, Thesis, Le Mans (1979).
11. A. Le Bail, H. Duroy, and J. L. Fourquet, *Mater. Res. Bull* **23,** 447 (1988).
12. G. M. Sheldrick, "SHELX76, A program for Crystal Structure Determination." Cambridge Univ. Press, London/New York, 1976.
13. G. M. Sheldrick, *Acta Crystallogr. Sect. A* **46,** 467 (1990).
14. G. M. Sheldrick, "SHELXL93," Program for the refinement of crystal structures." University of Göttingen, Germany.
15. "International Tables for X-ray Crystallography," Vol. IV, Kynoch, Birmingham, 1968.
16. H. F. McMurdie, M. C. Morris, E. H. Evans, B. Paretzkin, W. Wong-Ng, and C. R. Hubbard, *Powder Diffr.* **1,** 40 (1986).
17. A. Le Bail, Unpublished ARIT4 Program, Univ. du Maine, France.
18. G. Caglioti, A. Paoletti, and F. P. Ricci, *Nucl. Instrum. Methods* **3,** 223 (1958).
19. H. G. v. Schnering and P. Blekmann, *Naturwissenschaften* **55,** 342 (1968).
20. G. Knoke, W. Verschaften, and D. Babel, *J. Chem. Res. (S)* 213 (1979).
21. S. Andersson and J. Galy, *Acta Crystallogr. Sect. B* **25,** 847 (1969).
22. Y. Gao, J. Guery, and C. Jacoboni, *Eur. J. Solid State Inorg. Chem.* **29,** 1285 (1992).
23. A. Hemon, Thesis, Le Mans 1991.
24. J. Kanamori, *J. Phys. Chem. Solids* **10,** 87 (1959).
25. J. B. Goodenough, *in* "Magnetism and the Chemical Bond." Interscience–Wiley, New York, 1963.
26. L. J. deJongh and A. R. Miedema, *Adv. Phys.* **23,** 1 (1974).
27. L. Holmes, M. Eibschütz, and H. J. Guggenheim, *Solid State Commun.* **7,** 973 (1969).
28. J. M. Greneche, Université du Maine, Le Mans, France, private communication.
29. M. Eibschütz, L. Holmes, H. J. Guggenheim, and D. E. Cox, *J. Phys.* **32,** 759 (1971).
30. M. Eibschütz, L. Holmes, H. J. Guggenheim, and D. E. Cox, *Phys. Rev. B* **6,** 2677 (1972).
31. D. E. Cox, M. Eibschütz, H. J. Guggenheim, and L. Holmes, *J. Appl. Phys.* **41,** 943 (1970).